Experimental Investigation on Blast Response of Cellular Concrete

Weimin Nian[a], Kolluru V.L. Subramaniam[b1], and Yiannis Andreopoulos[c]

[a] Project Structural Engineer, DeSimone Consulting Engineers, New York, NY 10011, U.S.A.

[b] Department of Civil Engineering, Indian Institute of technology Hyderabad, Hyderabad, Telangana, INDIA 502205

[c] Mechanical Engineering Department, City College of the City University of New York, New York, NY 10031, U.S.A.

Abstract

A test setup consisting of a shock-tube with an instrumented short rod is developed for investigating the blast response of cellular concrete foams. In the shock tube facility, blast pressure wave is generated by the rupture of a notched Aluminum membrane. An instrumented rod is calibrated for measuring transmitted stress from the cellular foam. Experiments are conducted on brittle cellular concrete foam, which exhibits non-linear stress-strain behavior associated with crushing of the cellular structure and subsequent densification. Crushing is initiated when the stress exceeds the crushing strength and continued crushing produces an upward concave stress-strain curve leading to densification of the material. Foams with two

[1] Corresponding Author: Department of Civil Engineering, Indian Institute of Technology Hyderabad, Hyderabad, A.P., 502205, India. Email: kvls@iith.ac.in, Tel: +91-40-2301-6093; Fax: +91-40-2301-6032

different crushing strengths are evaluated. The influence of length of the foam is investigated. For an applied blast pressure amplitude which is higher than the crushing strength of foam, the wave structure in the foam consists of an elastic precursor wave followed by a compaction front which produces crushing of the cellular structure of the material. From the experimental investigation, the existence of a critical length for completely attenuating the applied blast pressure wave is established. For a given blast pressure loading, when the length of foam is larger the critical length, the applied blast pressure wave is transmitted as a rectangular pulse of nominally constant magnitude, which is slightly higher than the crushing strength of the foam. The foam is compacted without significant densification. The critical length depends on the crushing strength of the foam and the blast pressure amplitude and duration. If the length of foam is smaller than the critical length, there is an enhancement in the transmitted stress amplitude. If the length of foam is significantly smaller than the critical length, the transmitted stress is enhanced to a magnitude higher than the applied blast pressure amplitude and the compaction of foam leads to significant densification of the material.

Keywords: Blast; Shock; Cellular; Foam; Attenuation.

Introduction

Cellular materials possess energy-absorbing properties and are widely used as protective materials in applications such as improving crash worthiness [Gibson and Ashby 1999]. The successful use of these materials in mitigating impacts has drawn the attention of structural community towards the development of blast mitigation strategies. Use of sacrificial claddings when placed in the path of an incoming blast pressure wave alter the blast wave characteristics and reduce the stress transferred to the structural element to mitigate the impact of a blast pressure wave have been explored [Guruprasad and Mukherjee 2000]. The available information in the literature is sparse and not very consistent. Some experimental evidence and results from numerical simulations suggest the possibility of stress enhancement, rather than mitigation, in the substrate material when foam is placed in front.

The available experimental evidence indicates that both flexible polymeric and rigid aluminum foams produce pressure enhancement when subjected to shock loading. Shock pressure loading consists of a shock front followed by constant pressure and is associated with a linearly increasing impulse input with time. The pressure enhancement by foams was first shown for flexible porous material; the stress transferred at the back wall due to a planar shock wave reflected off the front face of the foam exceeded the pressure obtained without the porous material [Monti 1970]. These findings were later confirmed by experimental studies on the interaction of shock waves with very low density flexible polymeric foams; from polyurethane foam [Ben-Dor 1994 and Gvozdeva 1985] and using open-celled polymeric foams [Skews 1991 and 1993]. The polymeric foams used in these experiments had very high porosities (in the range of 90% and higher) and were able to rebound after the loading was removed. The transmitted stress from the head on collision of a planar shock wave to an elastic substrate through an open celled rigid porous material has also been shown to exceed the stress magnitude obtained from direct shock wave incidence on the substrate [Levy et al. 1993, Kamyab et al 2010]. Experiments with the use of metallic (Alumina matrix) and brittle (Silicon Carbide matrix) foams were confined to studying the response at shock pressure amplitudes which do not produce significant deformation of the solid skeleton. The extension of results for metallic and brittle foams at pressure amplitudes which would produce irreversible compaction, are not clear.

Loading associated with a blast pressure wave has a decaying pressure profile, which follows the sudden pressure rise produced by the leading shock front. Blast pressure loading is of a short duration and is associated with a finite impulse input. Therefore, extension of the findings from shock loading to the case of transient loadings with finite impulse is not yet clear. Limited results on stress amplification by soft foams for blast loading are available. In a study on the thoracic visceral injury from blast loading, it was found that the transmitted overpressure from air to the anechoic water chamber is enhanced significantly by a soft foam layer [Cooper et. al. 1991]. The results indicated that a soft foam layer attached to substrate may produce a higher level of damage in the protected object.

The experimental results on the use of metallic foams obtained from studies involving impact have shown the benefit of using foam in providing energy dissipation [Tan et al. 2005, Reid and Peng 1997]. It should however be noted that there is a fundamental difference in the nature of loading associated with impact and blast pressure. In an impact, the energy delivered to a solid substrate by a projectile travelling at a given velocity, is a fixed value but the stress transmitted at the interface can vary depending on the materials in contact. The loading history produced by an incident blast wave at different solid substrates is always the same (neglecting the effect of the fluid solid interaction) but, the energy transferred to the solid substrate varies depending upon the stiffness of the substrate and is larger for softer material [Subramaniam et al. 2009, Nian et al. 2010].

Experiments involving blast loading with the use of metallic and brittle foams have been confined to studying the interaction at blast pressure amplitudes which do not produce any significant change in the structure of the foam and deformations of the solid skeleton are limited to elastic deformations [Ben-Dor et al. 1994, Levy et al. 1995, Standley et al. 2002]. These studies were limited to understanding the change in the characteristics of the pressure wave upon transmission through the porous matrix. Experimental results on the blast response of aluminum foam panels, which undergo compaction showed that the addition of the foam panels increased the energy and impulse transferred to a structure [Hanssen et al. 2002]. The blast pressure wave obtained from an explosive charge was used. While the predictions of transmitted stress considering irreversible compaction of the material indicated a decrease in transmitted pressure to the face of the pendulum, these could not be verified since the applied blast pressure and the pressure transmitted to the substrate were not measured in the experiments. The increase in transmitted impulse was attributed to the geometric effect associated with the continuous change in the shape of the initially plane panel surface into a double-curved shape.

The available information consisting of successful use in mitigating impact using foams which undergo irreversible compaction do not provide sufficient indication about the application of foam in mitigating blast loading. The blast test results available in the literature [Cooper et. al. 1991 and Hanssen et al. 2002] are also not helpful since the stress transmitted from the foam to the solid substrate, which is critical to understand the behavior of foam in blast mitigation, were not measured. Careful experiments on blast response of foams obtained from experiments with well-defined input blast pressure waves, which would lead to a fundamental understanding of the behavior of foam, are currently not available.

In this study, an experimental investigation of the one-dimensional dynamic response of cellular concrete foams subjected to blast pressure loading was conducted. Cellular concrete is a class of brittle matrix foam, which exhibits compaction associated with crushing of structure. A shock tube was used to generate controlled blast pressure loading of different amplitudes and durations. Instrumentations for measuring the blast pressure history applied at the front end (loaded end) of the foam and the stress transmitted to a solid substrate through the foam (transmitted stresses) were developed. Cement foams of different densities and different lengths were evaluated for different blast pressure loadings. The deformation of the cement foam bars after application of the blast pressure loading was also recorded.

Cellular Concrete Foam

The cellular concrete foam has a cementitious matrix and a cellular structure consisting of large entrained porosity in the form of uniformly distributed air cells. The air cells are introduced by mixing a stable, voluminous, micro-bubbled foam into cement paste. The porosity of the mix is varied by controlling the volume of foam mixed into the cement paste. After setting, when the cement paste gains strength, the cementitious matrix develops a cellular structure. The bubbles in the foam form disconnected pore space.

The cellular concrete foams used in this study were made using cement paste with a water to cement ratio (by mass) equal to 0.55. The cement paste was prepared by mixing cement and water in a paddle mixer. Polypropylene fibers (Stealth® e3 micro-reinforcement, classification D700/800) were also added to the cement paste. Approximately, 10 grams of fibers was used for each 5 kg of cement paste. The foam was generated with a foam generator (shown in Figure 5.5) using a commercially available foaming agent. MEARLCRETE® FOAM LIQUID produced by Cellular Concrete LLC which is an aqueous concentrate of a surface-active Polypeptide-Alkylene Polyol condensate, specially formulated to yield tough, stable, voluminous micro bubbled foam. The foaming agent was diluted in water at the recommended dosage and mixed with air in the foam generator. The foam was then hand mixed with the cement paste and cement foams with two different wet cast densities equal to 432 kg/m^3 and 528 kg/m^3 were produced by varying the volume of foam added to the cement paste. Cylindrical samples with diameter equal to 44 mm were prepared using acrylic molds. The inner surface of the mold was lined with a Teflon paper. The paste with the entrained foam was poured into the mold in layers and gently tapped on the sides to ensure proper placement. After 7 days, the foams were demolded and left to dry in the laboratory environment (maintained at 23 ^oC and 50% RH). The dry densities of the foam after 7 days were equal to 384 kg/m^3 and 480 kg/m^3. The porosity of the cellular solid was determined using the relationship between the bulk density of the cellular material ($_{bulk}$) and the density of the solid matrix ($_{s}$) using the relationship, porosity $= (1 - {}_{bulk}/{}_{s})$. The $_{s}$ of the cementitious matrix was taken as 1400kg/m3 and the porosities of the foams with dry densities equal to 384 kg/m^3 and 480 kg/m^3 were estimated to be 73% and 65%, respectively.

A photograph of the cellular microstructure of a typical cement foam sample showing the dispersion of air cells is shown in Figure 1. A closed-cell foam structure with disconnected porosity can be identified. The walls of the porous network consist of hardened cementitious material. There was no moisture in the large pores of the cellular network. After 28 days of age (following casting) the quasi-static load response of the foams were obtained. Tests were performed by placing the foams inside an acrylic tube with inner and outer diameters equal to 44.5 and 50.8 mm, respectively. The acrylic tube was used to confine the material during compaction and to prevent the spalling of the material due to disintegration. The acrylic tube also allowed for viewing the deformation of the specimen during the test. The acrylic tube was instrumented with a strain gage to measure circumferential strains. To minimize the influence of friction in the relative motion between the foam and the tube during compaction, the cement foam was wrapped with two sheets of Teflon and a low viscosity oil was placed in the gap between the Teflon sheet and the inner wall of the acrylic tube. Load was applied to the foam using a steel cylinder which could slide inside the acrylic tube. The test setup with the acrylic tube and steel cylinder ensured a one-dimensional state of motion and to confine the material from disintegration. During the deformation, engineering strain was computed as the relative displacement between the two ends of the foam divided by the original length of the foam.

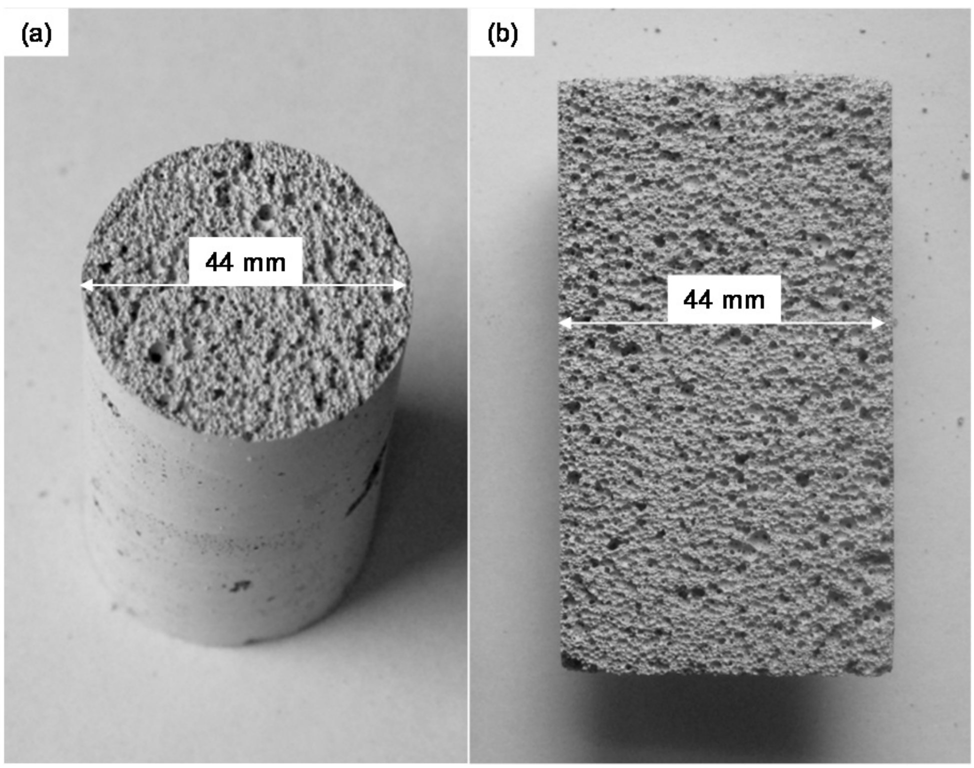

Figure 1: Photographs of the cellular concrete foam sample (a) cross-section and (b) a section along longitudinal axis

Typical quasi static load response of the foams is shown in Figure 2. Three distinct regions can be identified in a typical stress-strain curve of cellular concrete, namely the linear elastic response, the crushing plateau and the densification region. Initially, the behavior is linear elastic, with a slope equal to the Young modulus of the foam. The concave response is associated with the collapse of the internal structure and subsequent densification. The cell collapse is associated with brittle crushing of the cell walls. The collapse of cells and the densification of material produce a gradual upward concave stress-strain response with increasing slope as more cells are compacted. It should be noted that while engineering strain is calculated using the overall shortening of the entire length of foam, the local deformation in the material is non-uniform in the concave part of the load-response. Initially, the cell collapse progresses at roughly constant load where there is a large increase in strain associated with a small increase in stress, giving a stress plateau. Cell collapse continues until the opposing walls in the cells meet and touch, when densification causes the stress to increase steeply and approach that of the intrinsic material. The contribution of gas pressure to the measured strength properties was found to be insignificant and can be neglected [Nian et al. 2015, 2016]. For the measurements over the range of compaction evaluated in the study, the strains measured from the acrylic tube were insignificant. For the level of compaction considered in this study, the compaction is achieved at the expense of reduction of entrained porosity in the cellular structure. The compaction of the material, resulting in compression of the internal pore structure of the cementitious matrix, has not been considered in this study.

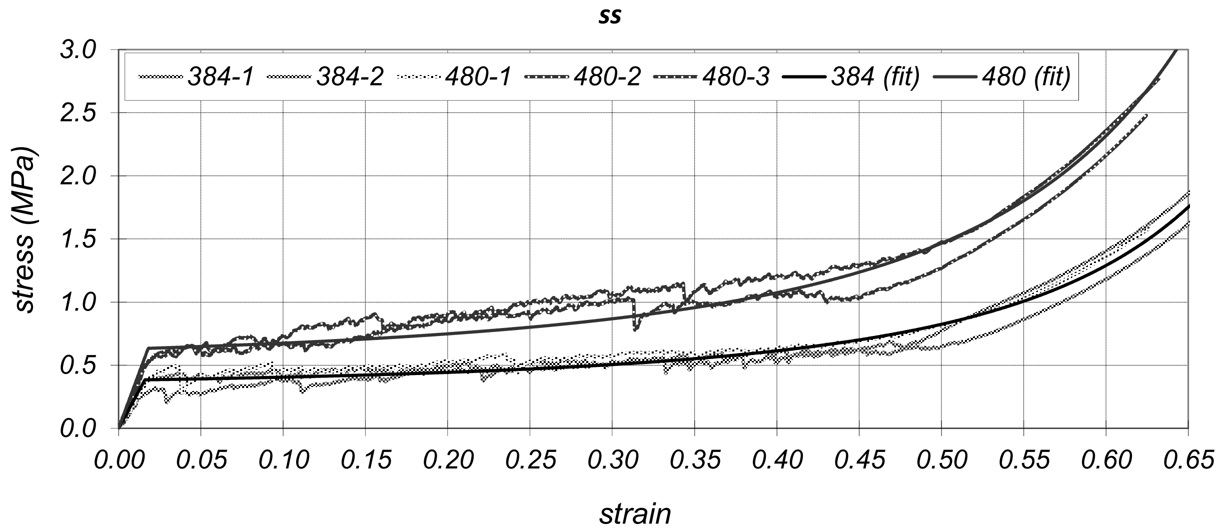

Figure 2: Quasi-static stress-strain curves of cellular concrete foams of different densities. 384 and 480 refer to dry densities of foam in kg/m^3.

Static stress-strain curves of cellular concrete foams were fitted using Equation (1) with the parameters given in Table 1.

$$\sigma = \begin{cases} E\varepsilon & \varepsilon \le \varepsilon_{po} \\ \sigma_{po} - AE\left(1-\varepsilon_{po}\right)^{\alpha} + AE\left(1-\varepsilon\right)^{-\alpha} & \varepsilon > \varepsilon_{po} \end{cases} \tag{1}$$

where E is the Young's modulus, $_{Po}$ is identified as the crushing strength and it marks the end of the linear elastic behavior, $_{Po}$ is the strain corresponding to $_{Po}$ ($_{Po}$ = $_{Po}$/E), is a constant greater than zero and A is a material constant. The fitted equation is shown in Figure 2 for comparison. The non-linear elastic response is initiated when the stress exceeds the crushing strength of the material, $_{Po}$. The average crushing strength of cellular concrete increases with an increase in the dry density of the cellular concrete; the crushing strength of cellular concrete with dry densities equal to 384 kg/m^3 and 480 kg/m^3 are equal to 0.384 MPa and 0.63 MPa, respectively.

Table 1: Parameters used for the fitted curves in Figure 2

Density kg/m^3	E MPa	A	po	po MPa	
384 (±4%)	24 (±9%)	1/350 (±35%)	0.016 (±12%)	0.384 (±12%)	2.9 (10%)
480 (±3%)	35 (±5%)	1/250 (±25%)	0.018 (±6%)	0.63 (±6%)	2.8 (10%)

Experimental Setup

A shock-tube was used for generating last pressure waves. The stress transmitted from the cellular concrete foam was measured using an instrumented short rod. During a typical test, the cellular concrete sample was attached in front of the instrumented short rod and blast pressure loading was applied on the front end of the foam sample while the transmitted stress from the back face of the sample was measured. Pressure transducers were installed in the shock tube along the path of the blast pressure wave to measure the applied pressure. Experiments were performed to determine the following: (a) the transmitted stress to a solid substrate as a function of the applied blast pressure loading; and (b) the deformation of cement foams due to loading from the blast pressure wave.

Shock tube for generating blast pressure waves

A schematic sketch and a photograph of the test facility are shown in Figure 3. The shock tube consists of a high pressure section (driver section) which is separated from the low pressure section (driven section) by a diaphragm. The shock tube has a circular cross-section and is entirely made of stainless steel. The driver section is 1.3 m in length and the inner and outer diameters are equal to 8.9 cm and 12.6 cm, respectively. The driver section is fitted with a screw-driven piston at the back end, which allows for varying the length of the pressurized part of the driver section. The back flange of the driver section is fitted with a threaded rod through its center, which is attached to a steel cylinder with a diameter equal to 8.9 cm. Grease is applied in the gap between the steel cylinder and the inner surface of the driver section to allow smooth motion of the cylindrical piston and to seal any gaps between the inner surface of the driver section and the cylindrical piston. The driven section is 3.3 m in length and the inner and outer diameters are equal to 4.5 cm and 7.2 cm, respectively. Pressure ports are machined at different locations along the length of the driven section for mounting pressure transducers. Pressure transducers are placed flush with the inner surface of the tube. The driven section (4.5 cm diameter) is connected to the driver section (8.9 cm diameter) with a 20 cm long nozzle. The diameter decreases smoothly from 8.9 cm to 4.5 cm over the length of nozzle. The nozzle is used to accelerate and increase the Mach number of the flow.

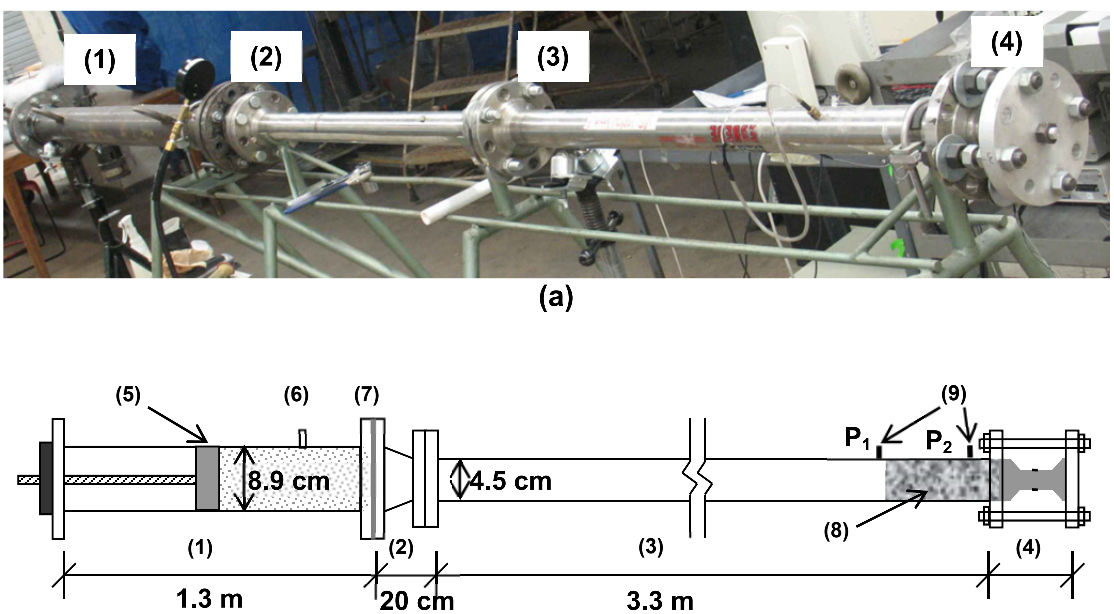

(a)

(b)

Figure 3: Shock tube test facility: (a) photo and (b) schematic diagram. 1) driver section; 2) nozzle; 3) driven section; 4) instrumented step rod and flanges; 5) screw-driven piston; 6) high pressure gas inlet; 7) diaphragm coupling; 8) cement foam sample; 9) pressure transducers P_1 and P_2.

Blast pressure wave generation

In a typical shock tube, the pressure wave is generated by the rupture of a diaphragm which is pressurized on one of its faces. The propagation of the different waves after the rupture is usually presented using an X-t diagram, as shown in Figure 4. Shock waves are generated by the sudden rupturing of the diaphragm as the pressure difference between the driver and the driven sections reaches a critical value. A compression wave generated by the sudden rupture travels downstream into the driven section and rapidly steepens to form a shock front. Simultaneously, a set of rarefaction (expansion) waves travel back into the driven section, reflect at the back end of the driven section as rarefaction waves and travel downstream in the same direction as the incident shock wave. According to Prandtl's relation, the sum of the particle velocity and local wave speed in the post shock flow is higher than the shock wave speed [Courant and Friedrichs 1999]. Thus, the sound speed at which the disturbance propagates in the post-shock flow is higher than the shock wave speed. When the reflected rarefaction waves, which travel faster than the shock front, catch up with the shock front, a blast pressure wave is generated. An incident blast wave consists of a leading shock front immediately followed by expansion waves, resulting in a decreasing pressures profile. The parameters, such as, the amplitude and the duration of the blast wave at the end of the driven section are controlled by varying the lengths of the driver and the driven sections and the pressures inside each section.

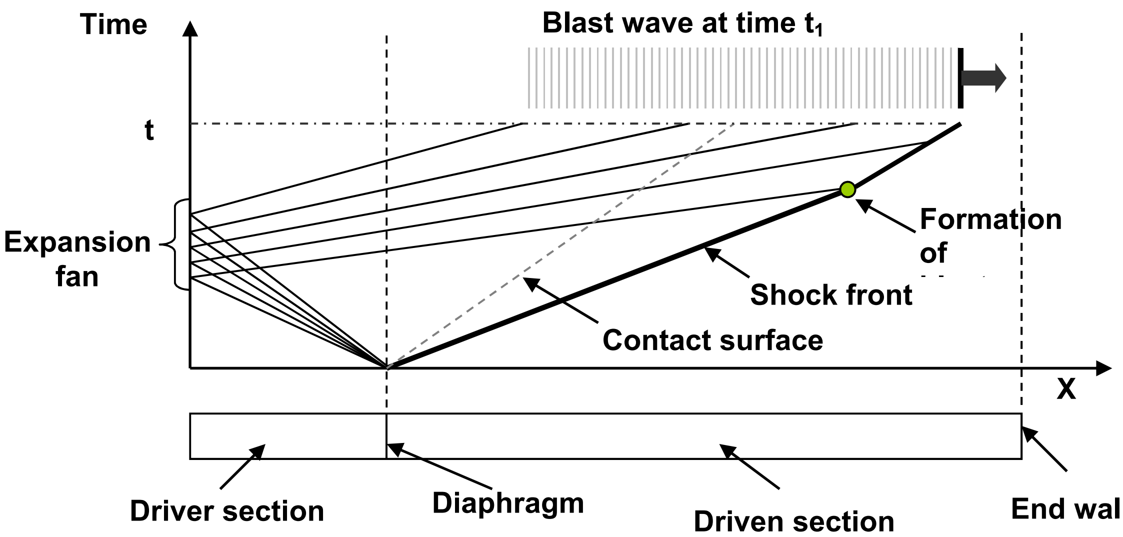

Figure 4: Formation of a blast pressure wave in the shock tube

Aluminum diaphragms were used for shock wave generation. Notches were machined on one of the faces of the diaphragm to ensure that it opened completely upon rupture. The initial pressure in the driver section at which the diaphragm ruptures was controlled by varying the depth of the notch in the diaphragm. Diaphragms made of Aluminum 6061-T6 with two perpendicular notches which intersect at the center, were used. The thickness of the diaphragm was equal to 1.6 mm and notches with different depths ranging from 0.8 mm to 1 mm were machined to obtain blast pressure waves with different amplitudes. The length of the driver section was adjusted by moving the piston within the driver section, to obtain the desired blast pressure characteristics. Compressed Helium was used for the high pressure gas in the driver section as it produces blast pressure waves of shorter duration when compared to air (or nitrogen). Pressure loading produced by the blast wave was measured using pressure transducers, placed close to the target end in the driver section of the shock tube. Different blast loads with pressure amplitudes ranging from 0.5 to 1.5 MPa and duration in the order of several milli-seconds (ms) were generated.

The shock tube facility provides the ability to control the pressure associated with the blast waves allows for a fundamental evaluation of the blast response of foams and also the determination of the material properties under high rates of loading. Such a facility offers a significant advantage in conducting blast studies when compared with the conventional methods which employ uncontrolled blast source from an explosive charge. In addition, the use of a shock tube allows for evaluating the material behavior without the interfering effects of debris.

Setup for measuring transmitted stress

An instrumented short rod with a stepped diameter was used for measuring the transmitted stress. The strain measured from the surface of the rod was related to the stress applied on the face of the rod. This is similar in principle as the technique to measure transmitted stress from transient loading in the conventional split Hopkinson pressure bar (SHPB) [Kaiser 1998]. A stepped rod, where the diameter of the rod at the location of strain measurement is reduced, provides a higher sensitivity (hence better signal to noise ratio) in measurements [Tan et al. 2005]. A short rod was used to overcome the limitation of length in the conventional Hopkinson pressure bar arrangement. In the conventional setup, the length of the pressure bar determines the useful duration of the signal. The maximum duration of the applied stress is limited by the time for reflection of the transmitted wave from the back end of the rod. For recording blast pressure signals with durations on the order of 10 ms, the length of the rod required in such a setup would be excessive (on the order of 25 meters) and hence, impractical.

In the short stepped rod, multiple reflections of stress waves form both ends and at the edges would occur within the duration of an applied stress pulse and the stress at a given location would be the result of superposition of the applied stress pulse and the reflected waves. The reflected waves would produce oscillations in the measured stress on a time scale associated with the time of travel for the waves over the length of rod. For a short rod, the time scale associated with the oscillations can be made significantly smaller than the time scale associated with the applied loading. In this case, the applied pressure can be separated by filtering the high frequency variations associated with the wave reflections.

In the experimental setup, the overall length of the instrumented short rod was selected such that the time scale associated with the oscillations was on the order of 10-100 s, while the blast pressure duration was in the range of 10 ms. The diameter of instrumented short rod was decreased from 44.5 mm at the loaded end to 19.2 mm at the measuring locations. The validity of using measured strain from the instrumented short rod by separating the contributions of the oscillations produced by reflections was confirmed using numerical simulation. In addition, the instrumented rod was calibrated against applied blast pressure signals. The transmitted stress recorded by the instrumented short rod when a blast wave is directly applied on the face of the rod was used for this purpose.

A schematic sketch of the instrumented short rod is shown in Figure 5. The instrumented short rod fitted perfectly inside the driver section of the shock tube and was fixed to a large aluminum plate at the other end. The aluminum plate was connected to the end flange of the shock tube using four threaded bolts. The sample to be tested rested against the face of the short rod. Four strain gages are placed 90 degrees apart around the perimeter in the middle of the short rod. To reduce the influence of the bending effect, misalignment of the fixture and asymmetric loading, the average of the four strain gages was recorded.

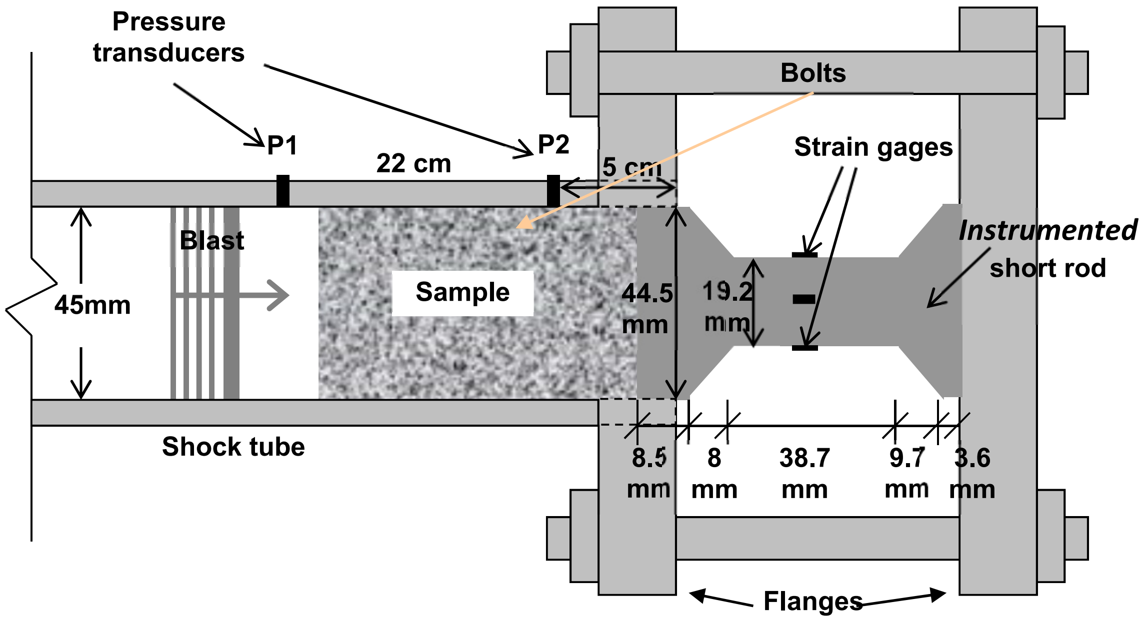

Figure 5: Schematic sketch of instrumented short rod with a stepped diameter used for measuring transmitted stress.

Measurement procedure for applied blast pressure and transmitted stress

The cellular concrete foam sample was attached to the instrumented rod using a quick setting epoxy. In order to reduce friction between the outer surface of the foam sample and the wall of the shock tube, the foam was wrapped with two sheets of Teflon paper. A low viscosity oil (viscosity = 1 cps) was placed in the gap between the Teflon paper and the wall of the shock tube. This was done to ensure lateral confinement to the sample during the compaction induced by the blast loading and to ensure a one-dimensional state of motion of the foam. The pressure sensor was used as to trigger the data acquisition.

Prior to putting the sample in the shock tube a ruler with markings spaced at 0.25 in. (6.4 mm) was marked on the surface using a permanent marker. All samples were photographed before and after the test. The overall change in length of sample after the test was recorded. In addition, the permanent strain was determined locally between the markings of the ruler.

Validation of the measurement procedure and calibration of the test system

The response of the instrumented short rod under a triangular pulse (representing blast loading) was simulated using the transient dynamic finite element analysis capability available in LS-DYNA. The purpose of this exercise is to validate the procedure for obtaining the applied pressure history using the measured strains from the short rod. A finite element model of a quarter of the short rod was developed and meshed using Ansys^{TM} (Version 10) as shown in Figure 6. The axis of the short rod was aligned with the Z-axis, while the X and the Y axes coincided with the planes of symmetry. A triangular forcing function with an initial peak value equal to 10 N and duration equal to 2 ms was applied on the all the nodes on the left face (with a normal in the Z-direction). The forcing function results in a triangular pressure pulse of $p_o = 7.46$ MPa and $t_B = 2$ ms on the narrow segment of the short rod (with a diameter equal to 19.2 mm) as shown in Figure 6. The other boundary conditions are such that the displacement of the cross section in XZ-plane was fixed in Y direction, the displacement of the cross-section in the YZ-plane was fixed in X direction and the displacement of the face at the right end was fixed in Z direction. The material properties of Aluminum alloy used for the short rod were $= 2700$ kg/m^3, $E = 69 \times 10^3$ MPa and Poisson's ratio = 0.3. The Solid 174, eight node quadrilateral element was used. The time step was determined as the time for the stress wave to across the smallest element factored by a 'Time step scale factor', which was set to be 0.9 for stability reason. The time step in the analysis was 0.15 s. The dynamic analysis was performed using LS-DYNA solver incorporated in Ansys™ (Version 10) package. The main solution methodology is based on explicit time integration [LS-DYNA theory manual 2006].

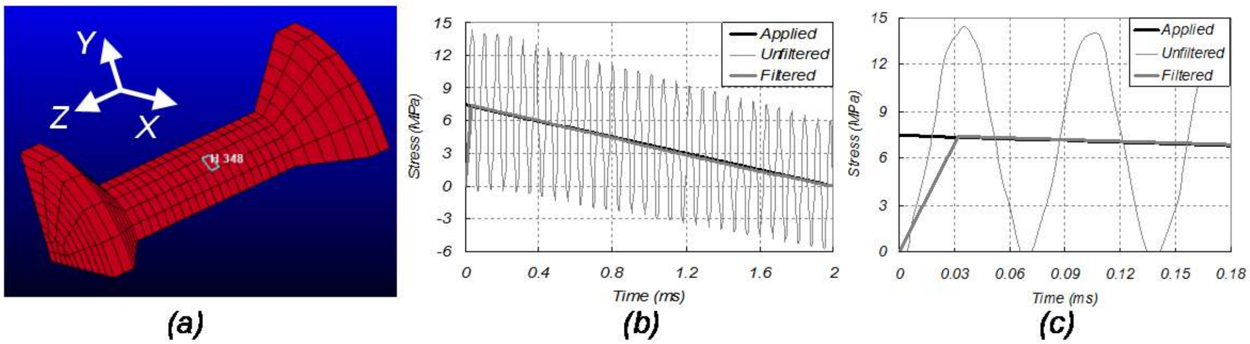

Figure 6 (a) Finite Element model of the short rod; (b) Stress history at a fixed location of the short rod due to an applied triangular pulse; Applied: applied stress at the loaded end, Unfiltered: unfiltered original stress response at the measured point and Filtered: filtered stress

The stress history of one element located on the surface of the rod, at the location corresponding to the location of the strain gauge on the specimen, is shown in Figure 6 (a). The stress response obtained from the dynamic analysis is shown in figure 6 (b). The applied pressure history is also shown in the figure for comparison. It can be seen that the stress at the specific location due to the applied triangular pulse shows a high frequency oscillatory response which is superimposed over a low frequency response with a triangular variation in time. It can also be seen that the initial stress rise produced by the wave propagation produces stress amplitude which is double of the actual applied stress. Clearly the oscillations are due to the multiple reflections of the elastic wave in the short rod, which produce a stress variation around the applied triangular pulse. The dominant period of the high frequency signal is approximately 66.6 s. The time period obtained from the numerical analysis compares favorably with the time estimated from a simple one-dimensional stress wave calculation over the length of the rod (equal to 68.5 mm) considering fixed-free conditions at the two ends. The time for one complete cycle for a compression wave can be estimated considering reflection at the fixed end (reflected as a compression wave) followed by a phase change produced by the reflection at the free end and the subsequent round trip over the full length of the rod, for the tension wave. Considering 1-D stress compression wave speed equal to 5055 m/s, this time period can be calculated as 54.2 s. The low frequency response recovered from the overall response using a low-pass, moving average filter over a time window equal to 66.6 s is also shown in Figure 6 (b). As is seen form Figure 6(b), the filtered response form the short rod compares favorably with the applied stress history. A close up view of the applied stress, the unfiltered stress and the filtered stress signals immediately following the rise is shown in Figure 6(c). It can be seen that the actual zero rising time of the onset of the applied triangular pulse has become 33 s for the filtered signal. This is due to the use of the low-pass, moving average filter over a time window equal to 66.6 s on the unfiltered signal.

Calibration of the instrumented short rod

The exact relationship between the recorded strain from the instrumented short rod and the stress at a given location would depend upon factors such as the gage factor of the strain gage, the material constants and the geometry of the rod. Considering linear elastic behavior and linear gage response, all these factors would result in a constant scaling factor for relating measured strain with stress at the location. In addition, the exact relationship between the applied stress on the face of the instrumented short rod and the measured stress at a given location on the rod depends upon the geometry and the elastic constants of the rod. Since the measured stress is linearly related to the applied pressure, this results in an additional scaling factor, which relates the measured and applied stresses. The combined effect of the geometric, material and instrumentation related factors would result in a calibration factor for relating the measured strain to the applied pressure, which can be determined experimentally. The stress measurement system was calibrated using a blast pressure input applied directly to the instrumented short rod. The pressure measured by the pressure gauges located adjacent to the front end of the instrumented short rod (P_2 as shown in Figure 3) corresponds to the applied stress input. The strain gauge output was calibrated against the applied pressure. The measured strain can therefore be converted to applied stress using the calibration factor.

The blast pressure loading applied on the face of the instrumented rod is shown in Figure 7(a). The applied blast pressure corresponds to the reflection of an incident blast wave at the face of the instrumented short rod and recorded using the pressure transducer P_2, located at a distance of 10 mm from the face. Figure 7 (b) shows the original unfiltered voltage signals obtained from the strain gages attached to the short rod. The high frequency oscillations associated with the wave reflections are clearly evident in the measured response (shown in the inset). The time period associated with the oscillations is measured to be 64 s, which agrees favorably with the value obtained from the numerical analysis. The low-frequency component of the original signal was obtained using a low-pass averaging filter with a time period equal to 64 s and is also presented in Figure 7(b). The calibration factor for the instrumented short rod was then obtained by matching the magnitude of the filtered voltage from the instrumented short rod with that of the applied stress obtained from the pressure gauge. The calibration factor was applied to the filtered voltage signal to give the stress history measured by the instrumented short rod and shown in comparison to the applied pressure history in Figure 7(a). The stress history measured by instrumented short rod and the applied pressure history measured by the pressure transducer are also shown over a shorter time interval closer to the initial rise in Figure 7(c). A good comparison between two time histories is observed in Figures 7 (a) and (c). The calibration using a real blast pressure wave shows that the measurement procedure provides an accurate estimate of the applied pressure history and the initial shock front is adequately resolved.

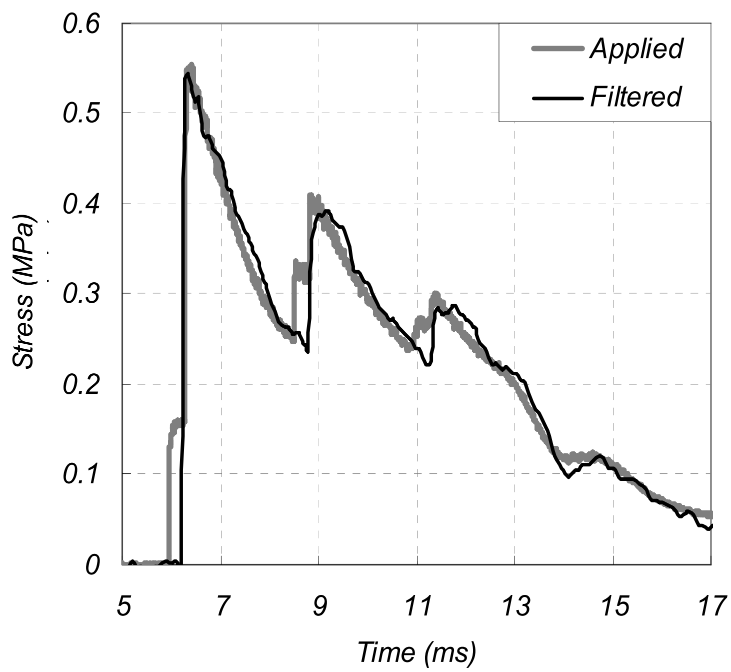

(a)

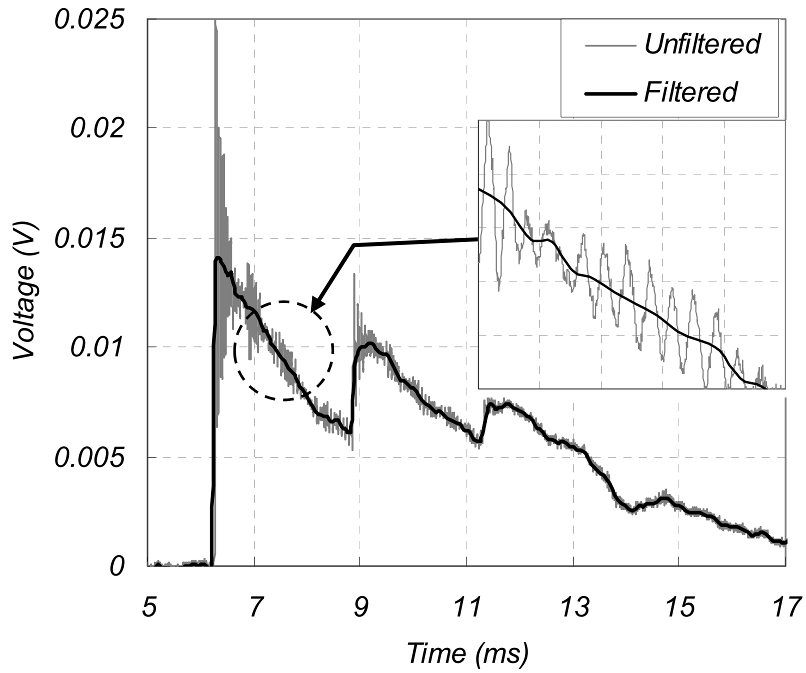

(b)

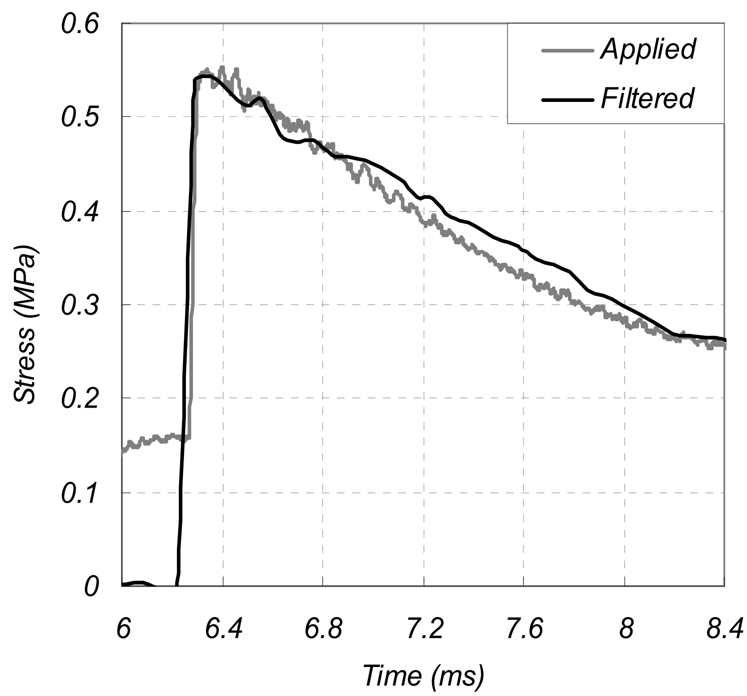

(c)

Figure 7 Stress history recorded by the instrumented short rod **when a blast wave strikes directly on it. (a) Applied pressure and calibrated filtered stress and (b) unfiltered and filtered signal from strain gages in voltage and (c) the close up view of the applied pressure and calibrated filtered stress.**

Comparisons between the calibrated stress signals from the instrumented short rod and the applied pressure for different blast pressure loads are shown in Figures 8 (a) and (b). The calibration constant determined from the results in Figure 7 was applied to the cases shown in Figures 8(a) and (b). The direct blast pressure measurements provide a validation for that the applied stress measurement using the calibrated strain measurements obtained from the short stepped rod.

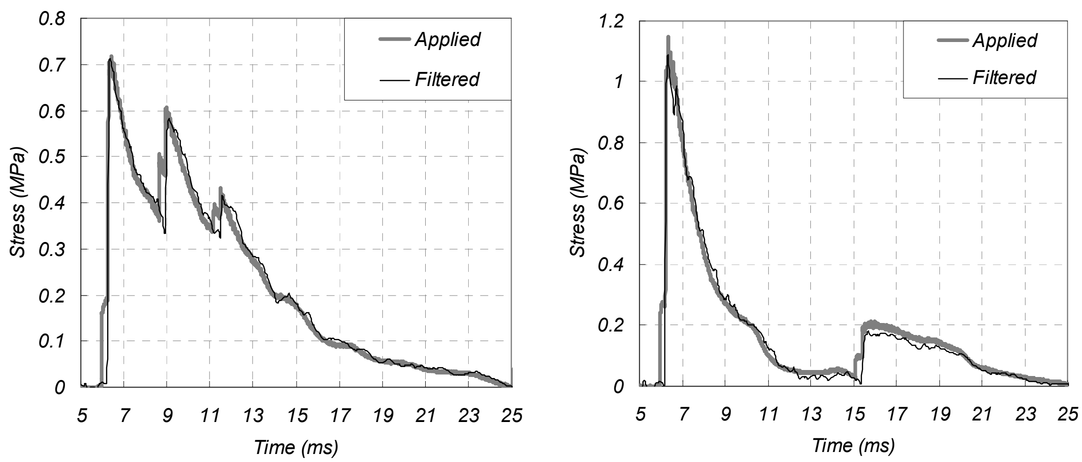

(a) **(b)**

Figure 8 (a) and (b): the applied pressure from the pressure transducer compared to the calibrated filtered stress from the instrumented short rod under different blast loads.

Experimental Results with Cement Foam

The results showing the applied and transmitted stress for 384 kg/m^3 and 480 kg/m^3 density foams are given in Figures 9 (a) and 9 (b), respectively. For each density, samples of varying length were subjected to blast pressure loadings of nominally similar amplitudes and durations. For the 384 kg/m^3 density foam, samples with three different lengths, L = 230 mm, 152 mm and 102 mm (designated as long, mid and short in Figure 9 (a)) were used in the test program. For the 480 kg/m^3 density foam, foam samples of lengths, L = 184 mm, 127 mm and 76 mm (designated as long, mid and short in Figure 9 (b)) were used in the test program. In all tests, the applied blast pressure amplitudes are comparable and nominally equal to 1.3 MPa, which is greater than the crushing stress of the foam; $_{po}$ is equal to 0.384 MPa and 0.66 MPa for foams with densities 384 kg/m^3 and 480 kg/m^3, respectively. From the results for both cement foams, it is immediately obvious that the transmitted stress depends upon the length of foam samples. Considering the response from the samples of the largest length for foam samples of both densities, the applied blast pressure loading is transmitted as a stress pulse of rectangular shape characterized by a nominally constant stress of a magnitude smaller than the applied pressure. The rectangular pulse has amplitude approximately equal to, but slightly higher than the crushing strength of the foam. As the length is decreased, there is an increase in the magnitude of stress, which follows the initial constant transmitted stress. The increase in the transmitted stress is very significant in the samples with shortest length; the transmitted stress amplitude is higher than the applied blast pressure amplitude producing stress enhancement for this case. The results indicate that when the length of the foam samples is sufficiently long there is a complete attenuation of the applied blast pressure to a stress level, which is slightly higher than the crushing strength of the foam. The length of the foam required to attenuate a given blast signal depends upon the crushing strength of the foam. On decreasing the length, there is an increase in the amplitude of transmitted stress. This suggests that there is a critical length of the foam (L_{cr}), which depends upon its crushing strength, which is required to completely attenuate the applied blast pressure loading. For the applied blast pressure loading, L_{cr} for the 384 kg/m^3 foam is smaller than 230 mm but larger than 152 mm. Similarly, for the 480 kg/m^3 foam, L_{cr} is smaller than 178 mm but larger than 127 mm.

When the length of sample is less than L_{cr}, the transmitted stress amplitude exceeds the crushing strength of the foam. When the length of the foam is significantly smaller than L_{cr},, the results indicate that there is a significant a stress enhancement, where the transmitted stress with the foam is higher than the stress directly applied by the blast pressure loading. This suggests that there is a minimum threshold length of the foam (L_{th}), smaller than L_{cr}, below which there is a stress enhancement to a value higher than the applied blast pressure amplitude. For the applied blast pressure loading, L_{th} for the 384 kg/m^3 foam is in the range {152 mm, 102 mm} and for the 480 kg/m^3 foam in the range {127 mm, 76 mm}.

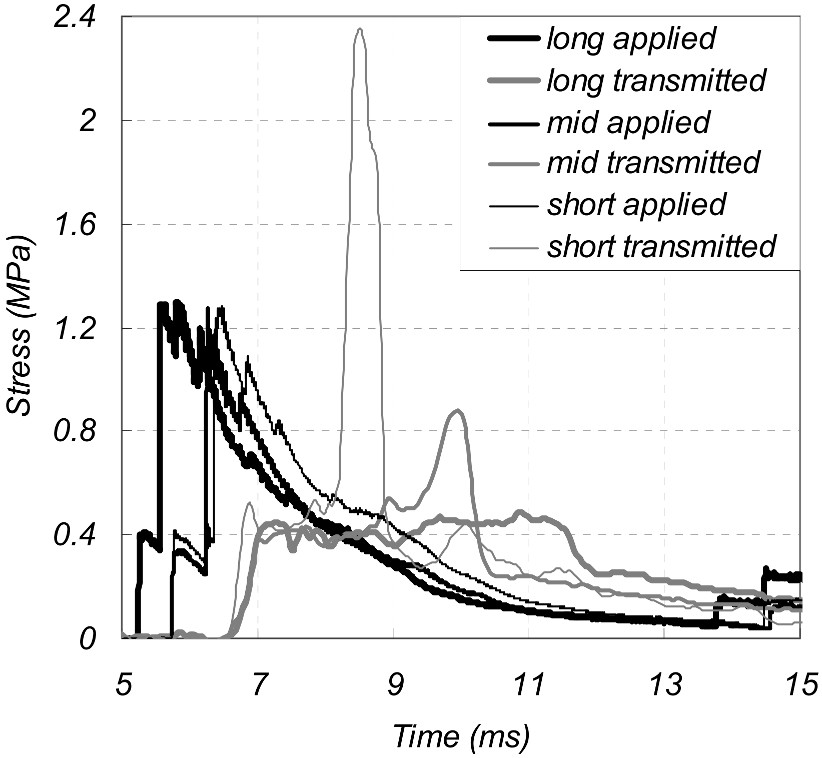

(a)

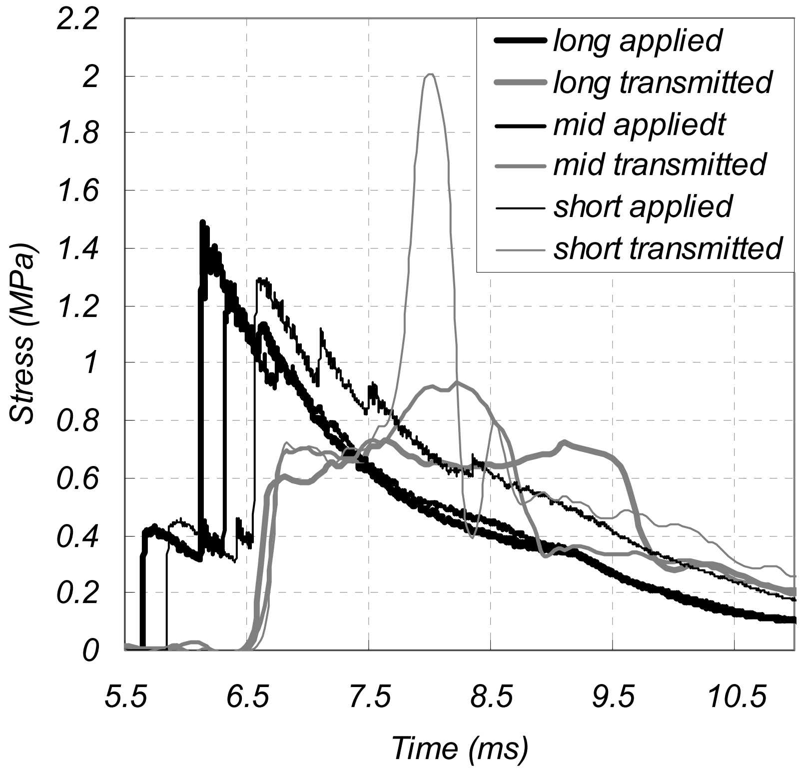

(b)

Figure 9: Applied blast pressure versus the transmitted stress subjected to similar blast loadings with different samples lengths (long/medium/short) for cellular concrete of the two densities, (a) lengths 230 mm/152 mm/102 mm for 384 kg/m^3 and (b) lengths 184 mm/127 mm/76 mm for 480 kg/m^3.

Analysis of Compacted Foam

Irreversible volumetric contraction was observed in all samples subjected to blast pressure loading. There was compaction of the material along the length of the sample, which was produced by the crushing of the cells. The length of the material compacted however, varied with the initial length of the sample. In samples of length larger than L_{cr}, compaction and crushing of cells was observed in material at both the loaded end and the transmission end. The material in the middle portion, away from the ends, was found to be relatively intact. In samples with length smaller than L_{cr}, compaction and crushing of cells was observed over the entire length of the foam samples.

Typical photographs of foam samples before and after testing are shown in Figures 10 and 12, respectively for the 184 mm and the 76 mm samples made with the 480 kg/m^3 density foam. For each sample, two opposite faces are photographed. In Figure 10, the initial length of the sample was, L=184 mm. In Figure 12, the initial length of the sample, L=76 mm. The engineering strain of the compacted foam along the length of the sample was obtained using the distance between two adjacent markings in the compacted material and is shown in Figures 11 and 13. In Figure 11 (184 mm long foam sample), it is observed that at the loaded end 80 mm foam is compacted with an irreversible strain equal to 0.45, and 60 mm foam is compacted at the transmitted end with an irreversible strain approximately equal to 0.3. The region between the two compacted portions remains relatively un-deformed. The result indicates that 184 mm is sufficient to attenuate the applied blast wave and it is larger than L_{cr} for the applied blast loading. In Figure 13 (76 mm cement foam), it is observed that at the entire foam is compacted and the average irreversible strain reaches up to 0.6. Therefore, the 76 mm does not provide sufficient length required to fully attenuate the applied blast pressure loading. Further, for length of foam significantly smaller than L_{cr} there is significant compaction of the foam, which is uniform across the length of the foam. The strain in the foam is in the densification part of the stress-strain response of the material. Therefore, L_{th} would represent the minimum length which would produce uniform compaction over the entire length of the foam to a value in the densification region of the foam.

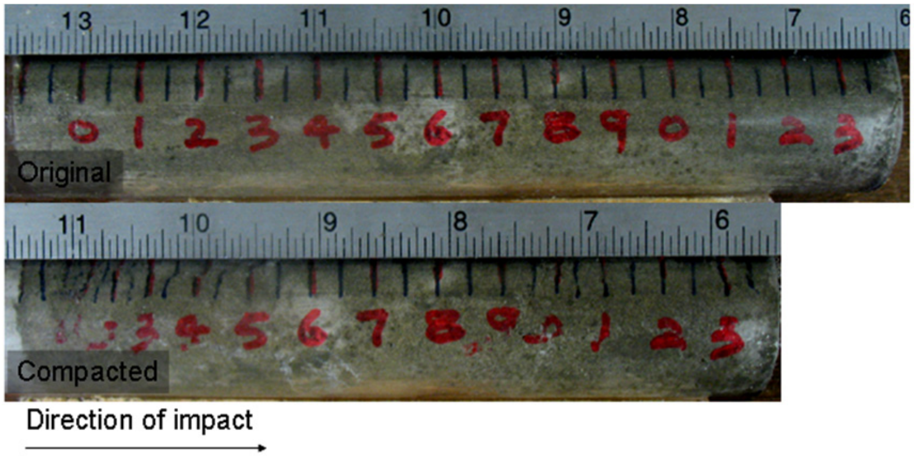

(a)

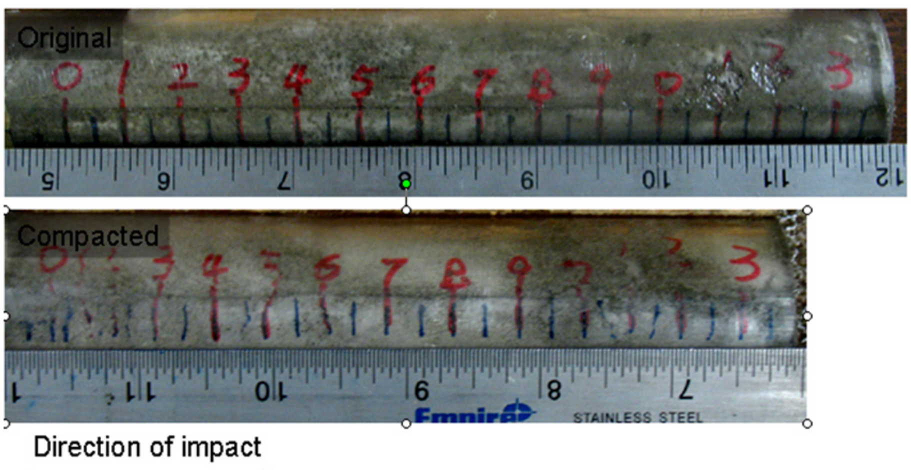

(b)

Figure 10: Deformation of L = 184 mm sample made with the 480 kg/m^3 cement foam before and after compaction (L > L_{cr} case), (a) face 1 and (b) face 2.

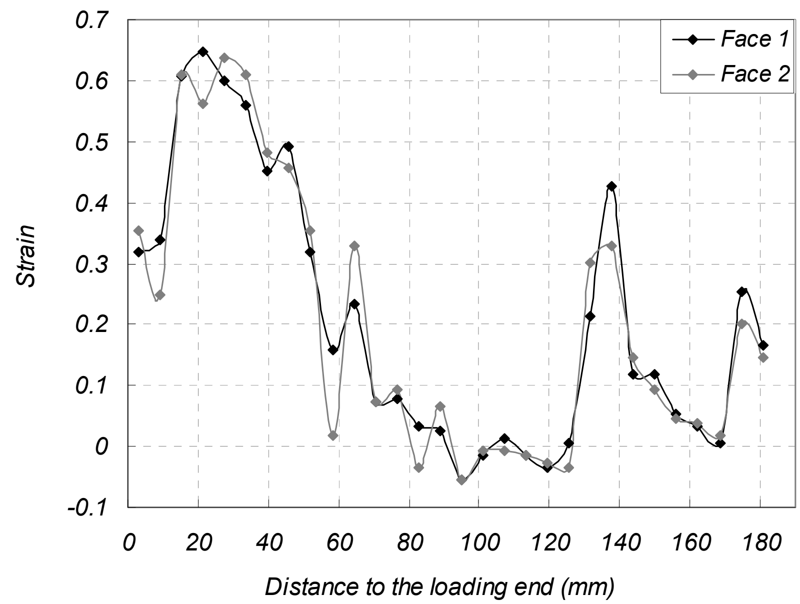

Figure 11: Engineering strain after compaction measured from Figure 10 for the foam with stress response shown in Figure 9

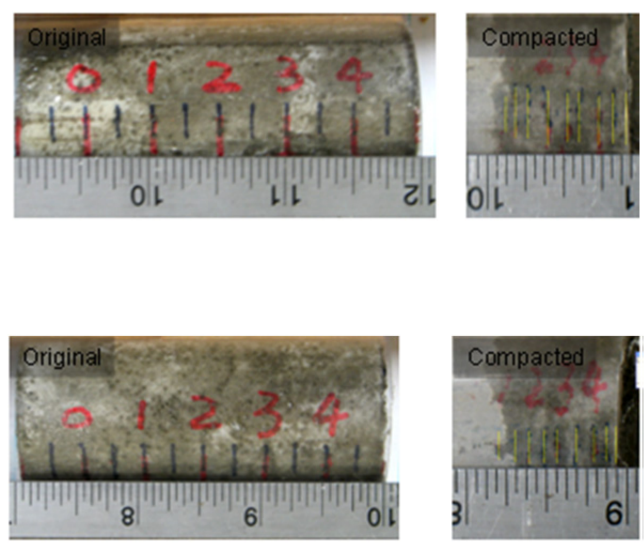

(a)

(b)

Figure 12: Deformation of L = 76 mm sample made with the 480 kg/m^3 cement foam before and after compaction (L < L_{th} case), (a) face 1 and (b) face 2.

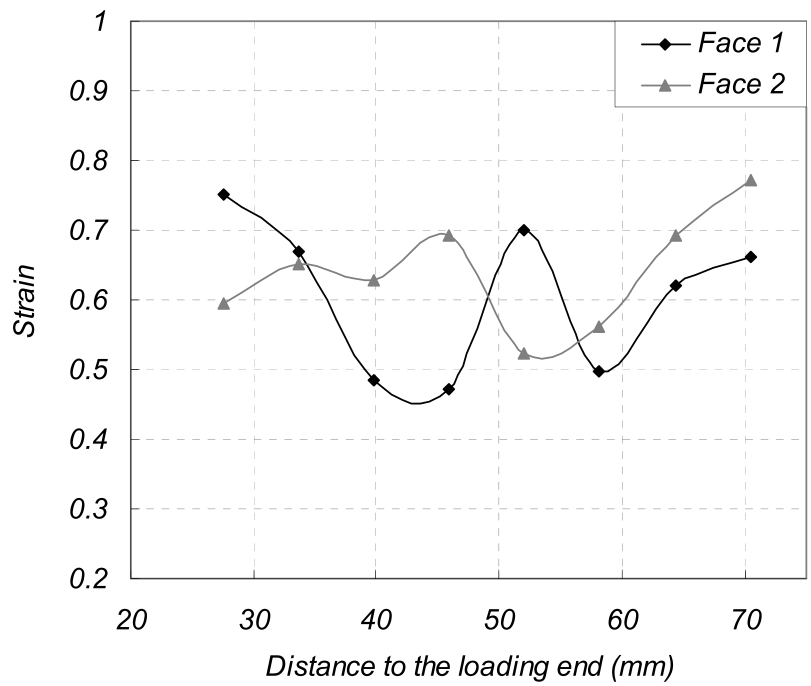

Figure 13: Engineering strain after compaction measured from Figure 12 for foam with stress response shown in Figure 9.

Discussion

The observed experimental response can be explained considering propagation of the stress waves through the cellular concrete. When the applied blast pressure wave produces an increase in stress at the loaded end beyond the crushing strength of the foam, stress wave(s) of different magnitudes are produced in the cellular concrete. An elastic wave which propagates at a speed predicted by the initial elastic modulus of the material travels into the material. Since the initial applied pressure amplitude is higher than the crushing strength of the cellular concrete, it also produces compaction of the cellular concrete immediately below the point of application of the applied stress. Two waves are thus formed in the material: (a) A faster elastic stress wave with amplitude equal to the crushing strength of cellular concrete; and (b) A slower compaction front, which produces densification of material in its wake. The elastic wave travels with constant amplitude as it propagates in the material. As the compaction front propagates in the material, there is a continuous decrease in its amplitude due to the energy dissipation provided by irreversible compaction of the foam. When the amplitude of the compaction front decreases to a value equal to the crushing strength of the cellular concrete, compaction of the material stops. The elastic wave propagates in the material and when it reaches the back end, reflection produces wave(s) travelling in the backward direction. There is an increase in the stress upon reflection from a substrate of higher stiffness; the stress increases above the crushing strength of foam. The stress transmitted to the substrate, which corresponds to the amplitude of the reflected pressure is therefore higher than the crushing strength of the foam. An elastic wave and a compaction front travelling in the reverse direction are produced after reflection. The compaction front produces densification till attenuation produced by compaction reduces its amplitude to the crushing strength of cellular concrete. The stress waves produced in the foam therefore produce compaction at both the front and the back ends of the foam. When sufficient length of foam is available, the material away from the ends remains uncompacted. The transmitted stress from the foam in this case is nominally higher than the crushing strength of the foam, since the reflection of the elastic wave of magnitude equal to the crushing strength, upon reflection from a substrate, which is stiffer than the foam produces a wave of magnitude larger than the incident wave.

In the case when the length of the foam is insufficient to completely attenuate the compaction wave produced by the incident blast pressure wave, the initial elastic wave of magnitude given the crushing strength of foam upon reflection from the substrate produces stress waves travelling back into the uncompacted foam. Since the stress rises above the crushing strength, both an elastic wave and a compaction front are produced. Subsequent stress history at the transmitted end is a result of a forward travelling compaction produced by the applied blast pressure loading and an elastic wave and a compaction front travelling in the reverse direction produced by the reflection of the elastic wave front from the back end. The reflection of the compaction front travelling in compacted material, from the back end results in a stress rise, the magnitude of which depends on the magnitude of the incident stress wave, densities of the material compacted foam and substrate and state of compaction of foam.

In a material which exhibits concave stress-strain response, the existence of the minimum length of material to attenuate the initial compaction front has previously been predicted using simplified a rigid-perfectly-plastic-locking (RPPL) idealization of the actual stress-strain response [Li and Meng 2002, Ma and Ye 2007, Nian et al. 2012]. In the RRPL idealization, the crushing and densification of the material occurs at a constant value of stress up to a fixed value of strain, following which the material exhibits a rigid behavior. The minimum length of the cellular concrete required to completely attenuate the applied blast pressure wave as it propagates down the length of the material, which is equal to the length of compacted foam on the front end, depends upon the impulse of the blast pressure wave and the crushing strength of the foam. The length of the cellular foam increases with an increase in the applied blast pressure impulse and decreases with the increase in the crushing strength of the material. The theoretical calculation shows that compaction ends when the impulse of the applied blast pressure wave equals the impulse of the transmitted stress wave with amplitude equal to the crushing strength of the material [Nian et al. 2015]. The experimental results indicate that the impulse of the applied blast pressure wave is conserved. The transmitted stress wave in the instrumented steel rod at the back end has the same impulse as the applied blast pressure loading [Nian et al. 2015].

Application of foams for blast protection applications therefore requires careful consideration. A low-strength foam can decrease the amplitude of the transmitted stress provided the length is larger than the critical length. For an applied blast pressure loading, if length is smaller than the critical length, the stress enhancement produced by the foam can increase beyond stress produced by direct incidence of the blast pressure on the substrate.

Summary and Findings

The results of the experimental investigation clearly show that for each applied blast pressure loading, there exists a critical length of cement foam, L_{cr}, which depends upon the cement foam density. When $L > L_{cr}$, the blast load applied to the foam bar is transformed into a rectangular stress pulse at the target end. The magnitude of the transmitted stress is nominally equal to the crushing strength of cement foam, $_{po}$, which is less than the peak blast pressure P_o, and therefore the cement foam reduces the peak stress delivered to the solid substrate to be protected. In $L>L_{cr}$ cases the compaction wave diminishes before reaching the solid substrate. The first rise and subsequent plateau of the transmitted stress is generated by the reflection of elastic precursor at the right boundary, the amplitude of which is solely determined by the characteristic of foam and is irrespective of the blast load. The amplitude is theoretically equal to $_{po}$ plus an overpressure Δc associated with the reflection of elastic precursor but Δc is typically negligible for foam type material.

When $L < L_{cr}$, there is a stress enhancement, where a second jump in the magnitude of the transmitted stress follows the initial rectangular shaped stress pulse. The stress enhancement is caused by the reflection of the compaction front from the surface of the substrate. If the length of the foam is significantly smaller than the required L_{cr}, the compaction in the material could reach a value in the densification phase of the stress-strain curve and the stress enhancement can be higher than the applied blast pressure amplitude.

Acknowledgements

The authors would like to acknowledge support from the National Science Foundation (Grant No. CMMI -0800307) during this study.

References

1. Ben-Dor G., Mazor G., Igra O., Sorek S. and Onodera H., Shock wave interaction with cellular materials, Part II: open cell foams; experimental and numerical results. *Shock Waves,* 1994, 3:167–79.
2. Cooper G.J., Townend D.J., Cater S.R., Pearce B.P., The role of stress waves in thoracic visceral injury from blast loading: modification of stress transmission by foams and high-density materials. Journal of Biomechanics 1991, 24(5):273–85.
3. Courant R., Friedrichs K.O., Supersonic flow and shock waves, Springer-Verlag 1976.
4. Guruprasad S. and Mukherjee A., Layered sacrificial claddings under blast loading. Part II Experimental studies. *International Journal of Impact Engineering*, 2000, 24: 975–984
5. Gibson, L.J., and Ashby, M.F., Cellular Solids – Structures and Properties, Progress Press, Oxford, England 1999
6. Gvozdeva L. G., Faresov Yu. M. and Fokeev V. P., Interaction of air shock waves with porous compressible materials. *Journal of Applied Mechanics and Technical Physics*, 1985, 26(3): 401-405.
7. Hallquist J.O., LS-DYNA Theoretical Manual, Livermore Software Technology Corporation, Livemore, California, 1998.
8. Hanssen, A.G., L. Enstock, and M. Langseth, Close range blast loading of aluminium foam panels, *International Journal of Impact Engineering*, 2002, 27: 593–618.
9. Hoff, G.C., New Application for Low-Density Concretes, ACI SP 29-11, 1971, 29: 181-220.
10. Kaiser M.A., Advancements in the Split Hopkinson Bar Test. M.S. Thesis, Department of Mechanical Engineering, The Virginia Polytechnic Institute and State University 1998
11. Kamyab W., Subramaniam K.V., Andreopoulos Y., Stress Transmission in Porous Materials Impacted by Shock Waves, *Journal of Applied Physics,* 2011, 109: 013523.

12. Levy A., Ben-Dor G., Skews B. W. and Sorek S., Head-on collision of normal shock waves with rigid porous materials. *Experiments in Fluids,* 1993, 15: 183–190.

13. Levy A., Sorek S., Ben-Dor G. and Bear J., Evolution of the balance equations in saturated thermoelastic porous media following abrupt simultaneous changes in pressure and temperature. *Transport in Porous Media*, 1995, 21: 241–268.

14. Li Q.M. and Meng H., Pressure-Impulse Diagram for Blast Loads Based on Dimensional Analysis and Single-Degree-of-Freedom Model, *Journal of Engineering Mechanics*, 2002, 128(1): 87–92

15. Ma G.W., and Ye Z.Q., Analysis of foam claddings for blast alleviation, *International Journal of Impact Engineering* 2007, 34 (2007) 60–70

16. Monti R., Normal shock wave reflection on deformable solid walls. *Mechanica* 1970, 4: 285-296.

17. Nian W., Subramaniam K.V., and Andreopoulos, Y., Dynamic compaction of foam under blast loading considering fluid-structure interaction effects, *International Journal of Impact Engineering*, 2012, 50: 29-39.

18. Nian W., Subramaniam K.V.L., and Andreopoulos Y., Experimental Investigation of Blast Pressure Attenuation by Cellular Concrete, *Materials Journal, ACI*, 2015, 112(1): 21-28.

19. Nian W., Subramaniam K.V.L., and Andreopoulos Y., One-Dimensional Numerical Framework for Shock Compaction of Cellular Foams, *Journal of Aerospace Engineering*, ASCE, 2016, (doi: 10.1061/(ASCE)AS.1943-5525.0000576)

20. Reid S. and Peng C., Dynamic uniaxial crushing of wood. *International Journal of Impact Engineering*, 1997, 19: 531–570.

21. Skews B.W., The reflected pressure field in the interaction of weak shock waves with a compressible porous foams. *Shock Waves*, 1991, 1: 205–211.

22. Skews B.W., Atkins M.D., and Seitz M.W., The impact of shock wave on porous compressible foams. *Journal of Fluid Mechanics*, 1993, 253: 245–265.

23. Tan P.J., et al., Dynamic compressive strength properties of aluminum foams. Part I—experimental data and observations. *Journal of the Mechanics and Physics of Solids*, 2005, 53: 2174–2205.

24. Standley E., Umnova O., Attenborough K., and Dutta P., Shock Wave Reflection Measurements on Porous Materials. *Noise Control Eng*., 2002; 50(6): 224-230

25. Subramaniam K.V., Nian W., and Andreopoulos Y., Blast Response Simulation of an Elastic Structure: Evaluation of the Fluid-Structure Interaction Effect, *International Journal of Impact Engineering,* 2009, 36(70): 965-974.